ICAS-98-3,11,2.

ICAS-98-3,11,1

A98-31572

Computation of Wind Tunnel Flow in Transonic Slotted-Wall Test Sections

Yngve C-J. Sedin
Saab AB, Future Products and Technology, Aeronautical Engineering, SE-58188 Linköping, Sweden
Nada Agrell
The Aeronautical Research Institute of Sweden, FFA, SE-16111 Bromma, Sweden

Abstract

An investigation of a discrete numerical slot flow model in slotted-wall test sections has been carried out. The background of the slot model is surveyed. Numerical simulations and wind tunnel tests have been performed in two different FFA wind tunnels, the 1.5x1.5 m^2 T1500 and the 0.5x0.5m^2 TVM500. The same model has been tested and calculated in both tunnels with the similar slots. The effect of closing the side walls in the TVM500 has been studied. Wall Mach number distributions and integrated forces are compared. The slot flow model works properly. The applicability of the small perturbation equation solved on a Cartesian grid needs further investigations. For complicated flows and high resolution on the test model a more advanced field equation solved on a body conform grid is needed. The same slot flow model could be used.

Introduction

Transonic flow is complicated from both physical and mathematical points of view. Wind tunnel wall-interference is of special interest at transonic speeds in particular when big models are tested. There are obvious reasons for using bigger test models than those conventionally tested today in existing tunnels. For big models empty test section calibration is losing its meaning. To master the new technique, one has to rely on some non-linear computational theory in order to quantify or to correct for the wall-model interaction. Other applications of computations are to help improve the design of test sections and to develop new test concepts and correction methods. It can equally be used to optimize tunnel run parameter settings minimizing wall interference. In any case the understanding of the main features of the interacting flow mechanisms is of utmost importance.

One classical concept diminishing the wall interference is to use longitudinal wall slots ventilating the test section through the surrounding plenum chamber. During the last 20 years, research work[1]-[14] has been ongoing more or less continuously in Sweden around this subject partly in cooperation between FFA and Saab. This work terminated in a discrete slot flow model. The mutual interaction between the slots and the interior is taking place in the test section.

Some years ago a new transonic slotted wall wind tunnel, the T1500 (1.5x1.5 m^2), was brought into operation at FFA. In connection with this a research program was set up at FFA testing the same model in two different tunnels, the new T1500 and a similar but smaller TVM500 (0.5x0.5m^2). The objective was to investigate the influence of model size and the effects of different slot shapes on the test results as well as to simulate the flow computationally. Some experimental and numerical results were reported earlier in Ref (14).

The background of the computational method has been described in a number of papers, some of them represented by Refs (2) (4) (5) (7) (8) (9) and (11). Other researchers at NASA Langley and McDonnell A/C Co have addressed the wall interference problem e.g. in Refs (15) and (16). In particular Al-Sadi[16] has performed extensive investigations of the same method as presented here with discrete slot simulations for a transport type aircraft model in the NTF .

The present paper reviews some of the background to the physical and mathematical slot flow model and shows computational results simulating the flow around a swept wing-body model. The model was tested both in the TVM500 and in the T1500 wind tunnels. The model cross sectional area was blocking less than 0.2% in the T1500, while in the smaller TVM 500 the blockage was as large as 1.7%. The rectangular test sections have basically 16 slots with 4 slots on each wall. To see the influence on the results of sealed side walls the smaller TVM500 was run with 8 slots by closing the slots on the side walls. Integrated model forces, wing pressure distributions and wall Mach numbers were recorded during the tests and partly compared with numerical simulations. The slot shapes were similar in the two test sections.

Flow models

The interior test section flow field is presently described by the non-linear small perturbation potential equation. The test model is in the computational domain surrounded by an unevenly spaced Cartesian grid and the boundary condi-

tions on the model are formulated within the framework of slender theory. On the test section walls and on the test model viscous boundary layer methods of integral type are used modifying the geometric inviscid boundary conditions. The slot flow model is basically founded on crossflow theory coupling the plenum chamber pressure with the interior of the test section. A boundary condition for the flow around the model is created when the plenum pressure is known. The fluxes through the slots are *a´ priori* unknowns and are parts of the solution.

The simple non-linear potential field equation can in principle be substituted by e.g. the Euler equations. The outer 'wall' boundary condition in the vicinity of the slots must then be reformulated as well as the upstream test section inflow to suit e.g. a time asymptotic solver.

Basic slot flow physics revisited

To simplify the coupled discrete interaction between the plenum chamber and the interior of the test section flow, it may be sufficient to look just at the convective crossflow part of the momentum equation in the center plane of the slot. In a longitudinal x-y symmetry plane the pressure gradient pointing into the slot then is

$$\frac{\partial p}{\partial y} = -\rho U \frac{\partial V}{\partial x} - \frac{\rho \partial V^2}{2 \partial y} + \ldots \qquad (1)$$

In Eq (1) p is the pressure and ρ is the density while U and V denote the downstream (x) and crossflow (y) velocities . Assuming that ρU and ρ are of the same order of magnitude as in the reference flow , two distinguished terms of different importance can be identified in Eq (1) . The first term, reflecting the streamline curvature, is dominant when the crossflow is $V \approx 0$ and the second term is dominant when $\frac{\partial V}{\partial x} \approx 0$. Roughly, inside the slot, the velocity V is geared-up inversely proportional to the wall openness ratio compared to the crossflow velocity approaching the wall from inside the test section. To estimate the crossflow velocity V in the slot flow region the slot volume flux per unit length is needed. This in order to couple the known plenum pressure to the interior of the test section by integration of Eq (1). In doing so an outer boundary condition can be established inside the test section for the test section flow around the test model. However, as the flux through the slot is not known *a' priori,* a prescriptive method must be iterative.

In Ref (8) an experimental transonic investigation presented some flow inside one of the slots of an octagonal test section with slots in all the corners. The test object was an axisymmetric parabolic arc body blocking 2.2 % of the tunnel. To show the importance of the different terms in Eq (1) some information is compiled in Figure 1 and Figure 2. The wall pressure in Figure 1 can roughly be said to be the outcome of integrating Eq (1) from the plenum chamber side, where the pressure is known, through the slot down to the vicinity of the slot inside the test section outside the close range of slot interaction. From the velocity inclination V/U and the wall pressure it is clear that the first term of Eq (1) is of special importance where the pressure is minimum and likewise the second term is of particular importance where the pressure is at its maximum. The integration of the first term of Eq (1) yields the dominant influence by the slot depth on the pressure difference across the slot. A deep slot is able to sustain a higher difference than a shallow due to the longer integration path. The existence of a returning streamline is obvious from V/U in Figure 1.

In Figure 2 some measurements of the axial velocity U in the center plane of the slot are shown in terms of U/U_i where U_i is the velocity just outside the slot entrance in the test section. The distribution at the slot exit line B reveals quite large velocity losses there.

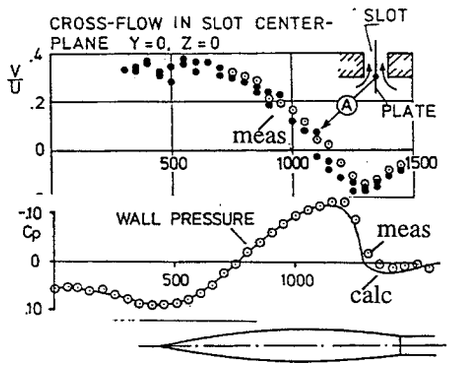

Figure 1 Streamline inclination V/U from oil-flow pictures along A at slot entrance; Wall pressure in between slots. Mach = 0.98.

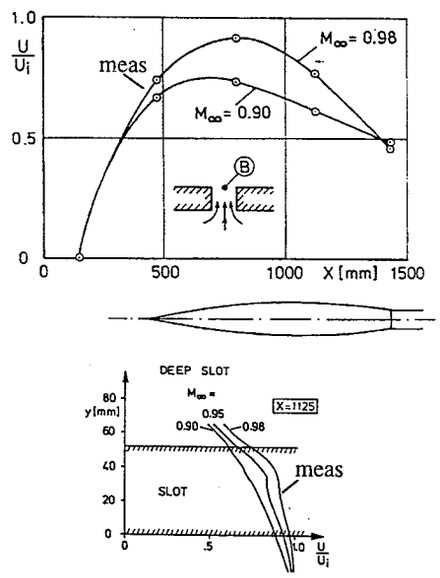

Figure 2 Axial velocity U/U_i measured along a line B at slot exit in plenum chamber; Axial velocity U/U_i through slot at a particular x.

However, it turns out that following a path in the slot that should be a natural candidate for imposing the constant plenum pressure the situation is a bit different. Hence, following the most upstream penetrating streamline until the intersect of B- then progressing along B until the first returning streamline starts at B- and finally then continue along this, the loss ratio U/U_i is ranging more modest values. An illustration to this is shown in Figure 3 where the velocity and mass density ratios along the mentioned path are shown. In this case the slot is more shallow than in Figure 2 reflecting that U/U_i is close to 1 where the slot is filled up with high momentum air. The range for U/U_i in Figure 3 is between 0.67-1.0.

In conclusion it can be said that an inviscid prescriptive slot theory must include viscous flow corrections or adaptions.

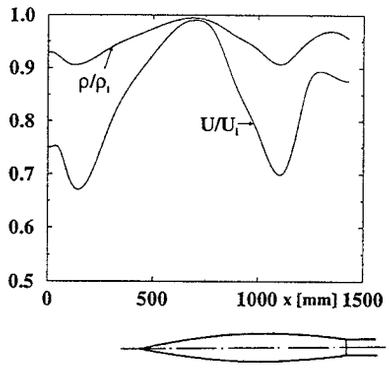

Figure 3 Measured velocity and density losses in slot along the path: *'Forward Streamline'-'Slot Exit'-'Returning Streamline'*.

Inviscid 2D inner crossflow slot theory

In Ref (2) a 2D crossflow potential theory was formulated for the slot flow. The velocity V in Eq (1) could then be estimated as function of the volume flux q through the slot to determine the pressure difference across the slot by integration of Eq (1). In Figure 4 the elements of the 2D flow model and the conformal mapping are shown

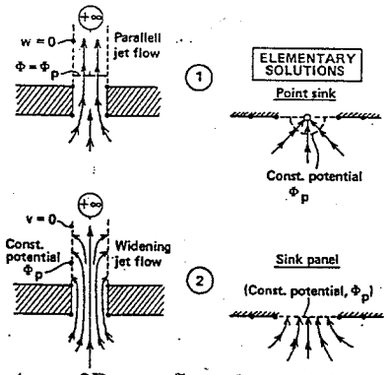

Figure 4 2D crossflow slot model (source -2*q*).

In principle two elementary solutions are building the flow. However in practice only No 1 is used, but the position for applying the plenum pressure is found where the two flows have got the same potential value on the plenum side.

Extended overall viscous slot flow model

In Ref (2) an overall slot flow model using the 2D inner crossflow potential was formulated and asymptotically matched to the global interior formulating an outer wall boundary condition for the interior. Based on experimental findings in Ref (8) the inner slot flow model was modified to take viscous slot flow losses into account. The overall model then came out as shown in Figure 5. Different flow scenarios can take place concerning the in and outflow from the slots with possible vortical separation or aperture like flow at slot inlet edges. A sheared flow can be observed in the slot center plane resulting in a velocity profile.

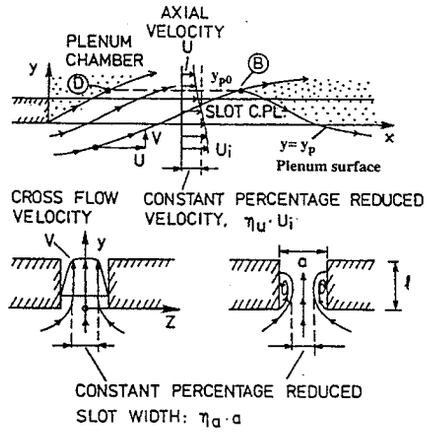

Figure 5 Overall viscous corrected slot model.

As a consequence of the experimental observations the inviscid slot flow model was corrected by two loss factors one for the axial velocity η_U and another for the slot width η_a. The important plenum surface y_p on which the quiescent plenum chamber pressure condition is imposed is traced in the model as a part of the solution. In Figure 5 this starts with the upstream penetrating streamline ending at location D, then progressing until B by jumping from streamline to streamline along a surface y_{p0} just outside the slot exit and then finally following the first returning streamline starting at B. The fast high-momentum test section air penetrating the slot might be split-up into two streams one continuing into the plenum chamber on its own and the other returning into the test section again together with an expanding bubble of quiescent plenum air.

Discrete slot flow equations

The discrete slot flow equations are applied one for each slot similar to what was done in e.g. Refs (7), (9). In comparison with the original viscous flow reduction model of

Ref (8) simplifications were imposed concerning the order of magnitude of the interior tunnel flow just outside the slot. In the viscous reduction scaling process the interior flow is assumed to be of the same order as the chosen reference flow labelling the wind tunnel test. The flow equations in the slot centerplane (see Figure 5) solving for the plenum surface and pressure difference across the slot are

$$\frac{dy_p}{dx} = \frac{q_s}{a_s}\mathcal{V} - E\frac{y_p}{a_s}\frac{da_s}{dx} \tag{2}$$

$$\Psi = q_s\left[Q - \frac{1}{\pi}\left(\frac{1}{2} + ln\left(\frac{4}{b}a_s\right)\right)\right] - \frac{E}{2}\frac{y_p^2}{a_s}\frac{da_s}{dx} \tag{3}$$

$$\frac{d\varphi}{dx} = -\frac{\rho_s}{\rho_r}\frac{U_s}{U_r}\left(\frac{d\psi}{dx} + \frac{1}{2}\frac{U_s}{U_r}\left(\frac{dy_p}{dx}\right)^2\right) - \delta \tag{4}$$

The potential φ is the perturbation potential at the matching distance outside the slot on the test section side where the unit step function $E=0$. When the slot is filled up with high-speed air the plenum pressure surface y_{p0} is defined:

$$\frac{y_{p0}}{a_s} = \frac{l}{a_s} + ln(2)\frac{\left(1 + 2\exp\left(-2\left(\pi\frac{l}{a_s} + 1\right)\right)\right)}{\pi} \tag{5}$$

The normalized velocity and potential functions $\mathcal{V}$ and Q in Eqs (2), (3) are results of the conformal mapping in Figure 4 and defined for unit slot width and flux, see in Refs (2), (11). The slot depth is denoted by l. The scaled viscous corrected variables are subscripted by s while the constant reference flow is denoted by subscript r. The scaled slot width, velocity and density become

$$a_s = a\eta_a \qquad U_s = U_r\eta_U \tag{6}$$

$$\rho_s = \frac{\rho_r}{\left(1 + \frac{(\gamma-1)}{2}M_r^2(1-\eta_U^2)\right)} \tag{7}$$

The plenum pressure coefficient δ and the definition of the approximate plenum Mach number M_p are as follows

$$\delta = \frac{(p_p - p_r)}{\rho_r U_r^2} \qquad M_p = M_r(1-(\gamma+1)\delta)^{\frac{1}{2}} \tag{8}$$

where M_r is the Mach number of the constant reference flow usually labelling the tunnel run. In fact in the present physical and mathematical model the plenum Mach number is the only fixed information which is available. The theory does not tell how this Mach number is achieved. In the real situation this is commanded to the control system and executed by operating the choke, the plenum suction device and possibly a flap at the end of the plenum chamber. The background information to the control system is usually found from empty tunnel calibrations.

Paying attention to the calculation of the slot flux per unit length passing in and out of each slot a wall strip of width b ($b>>a$) is discretely allocated to each slot on the wall as shown in Figure 6.

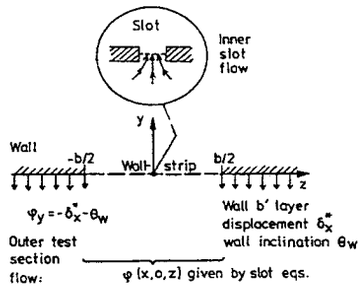

Figure 6 Discrete slot wall strip communicating with inner and outer flows ($b>>a$).

The slot volume flux q_s is only partly summed up by integrating the normal velocity v_n (coming from the interior test section) across the wall strip of width b. The total flux balance, however, is built from the interior test section flow (v_n) but also from the wall inclination θ_w and the boundary layer displacement thickness δ^* across the strip as follows

$$q_s = \frac{\rho_r}{\rho_s}\frac{U_r}{U_s}\left(\int_{-\frac{b}{2}}^{\frac{b}{2}} v_n dz + (b-a)\left(\theta_w + \frac{d}{dx}\delta^*\right)\right) \tag{9}$$

Test section field equation and wall boundary conditions

The test section flow equation is the non-linear small perturbation equation as follows

$$\left(1 - M_r^2\left(1 + (\gamma+1)\frac{\partial\phi}{\partial x}\right)\right)\frac{\partial^2\phi}{\partial x^2} + \frac{\partial^2\phi}{\partial y^2} + \frac{\partial^2\phi}{\partial z^2} = 0 \tag{10}$$

On the solid walls surrounding the slot strips the outleading Neumann condition for the potential ϕ is

$$\frac{\partial\phi}{\partial n} = -\frac{d}{dx}\delta^* - \theta_w \tag{11}$$

On the discrete wall strips, following the same procedure as outlined in Ref (7), the Dirichlet condition reads

$$\phi(x,0,z) = \varphi(x) - 4\frac{q_s}{\pi}\left(\frac{z}{b}\right)^2 + z\cdot\left.\frac{\partial\phi}{\partial z}\right|_{y=0,\,z=0} \tag{12}$$

The last term in Eq (12) is a correction for side wash while the potential φ is found in the slot centerplane by integrating the momentum equation resulting in Eq (4). The frame of reference (x,y,z) of Eq (12) is the local coordinate system shown in Figure 6.

The TSP method of Ref (17) was used to solve Eq (10). On the test model the no-throughflow condition with correction for boundary layer on the wing surface is applied within the theory of small perturbations.

Experimental setup

Wing-body test model

The considered swept wing-body test model is schematically shown in Figure 7. It has the full wing span of 0.4 m. It has been tested in the rectangular TVM 500 test section of cross section 0.5x0.5 m^2 and likewise in the test section T1500 with cross section 1.5x1.5 m^2. The average relative wing thickness is about 9 %. The inner wing leading edge sweep is 61.91° while for the outer main wing is 38.92 °.

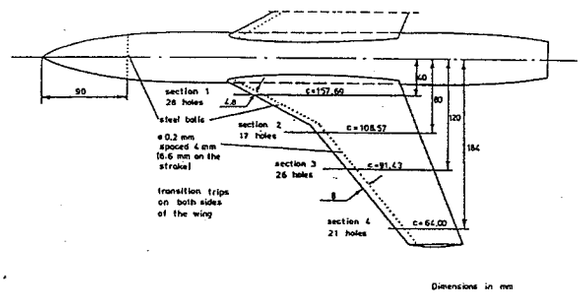

Figure 7 Swept wing-body test model PT8-99.

Test sections and relative model size

The relative model size as well as the half slot width shape in the TVM500 and the T1500 test sections are illustrated in Figure 8. The total wall ventilation in both test sections was 8.5%. The test section area blockage ratio was 1.7 % in the TVM500 while it was less than 0.2% in the T1500 test section. Both test sections were provided with 16 longitudinal slots with 4 on each wall. The slot width to slot depth ratio was at the test model x-location about a/l = 1.76. A schematic view of the cross section with slot locations and active wall pressure tap rows are shown in Figure 9. The TVM500 had parallel walls while the T1500 had the top and bottom walls diverging with about 0.003 radians to account for the wall boundary layer growth. In T1500 the model spanned 27% and in the TVM500 it spanned 80% of the tunnel width.

Computational Results

Calculated and measured effect of closing the side walls

To see the effect of closed side walls in the TVM500 test section reducing the total ventilation by one half, the slots with numbers 5 to 8 were closed (see notations in Figure 9). This resulted in two options with 16 slots distributed with 4 on each wall and 8 slots distributed only on top and bottom walls with 4 on each.

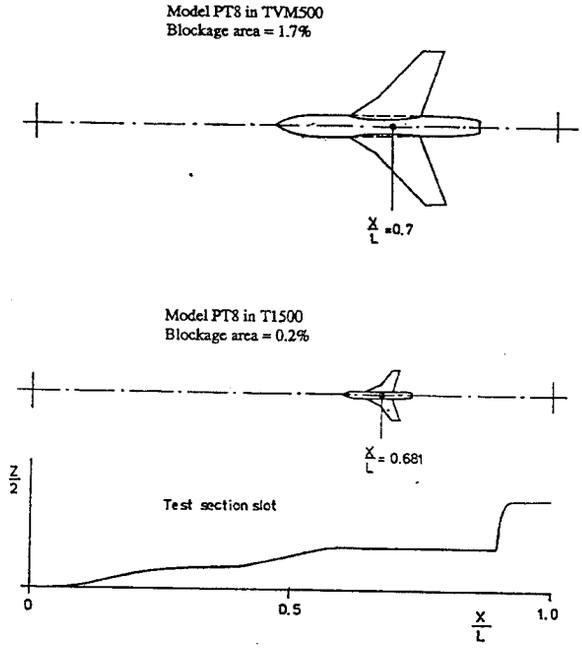

Figure 8 Relative model size of PT8-99 in TVM500 and in T1500 test sections; Slot half width shape distribution, a/2.

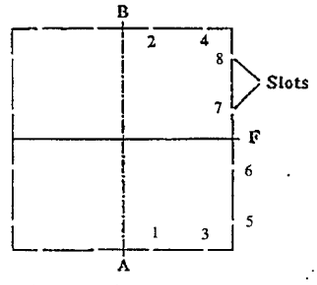

Figure 9 Test section cross sectional view; Slot locations 1-8 and pressure tap lines A,B,F .

In Figure 10 the calculated and measured wall Mach number distributions are compared for the two options. The Mach number is 0.9 and the angle of attack α=1°. The upper part of the figure is showing Mach along the centerline B of the top wall and the lower part along the centerline of the side wall at position F. The same trend is found both in experiment and in calculations, the Mach number at the entrance is reduced while the maximum Mach number is increased due to reduced ventilation. By reducing the ventilation for roughly the same wall flux condition created by the test model and about the same imposed plenum Mach numbers, the pressure difference across the slots will be increased due to decreased ventilation. As the crossflow velocity V inside the slot roughly is proportional to q/a, the consequence of reducing the ventilation is very clear from Eq (1) as a is the same at top and bottom walls while q is increased due to the sealing of the side walls . Considering

Mach at the entrance positions B and F for the case with solid side walls, a spanwise Mach gradient becomes obvious in both experiments and calculations.

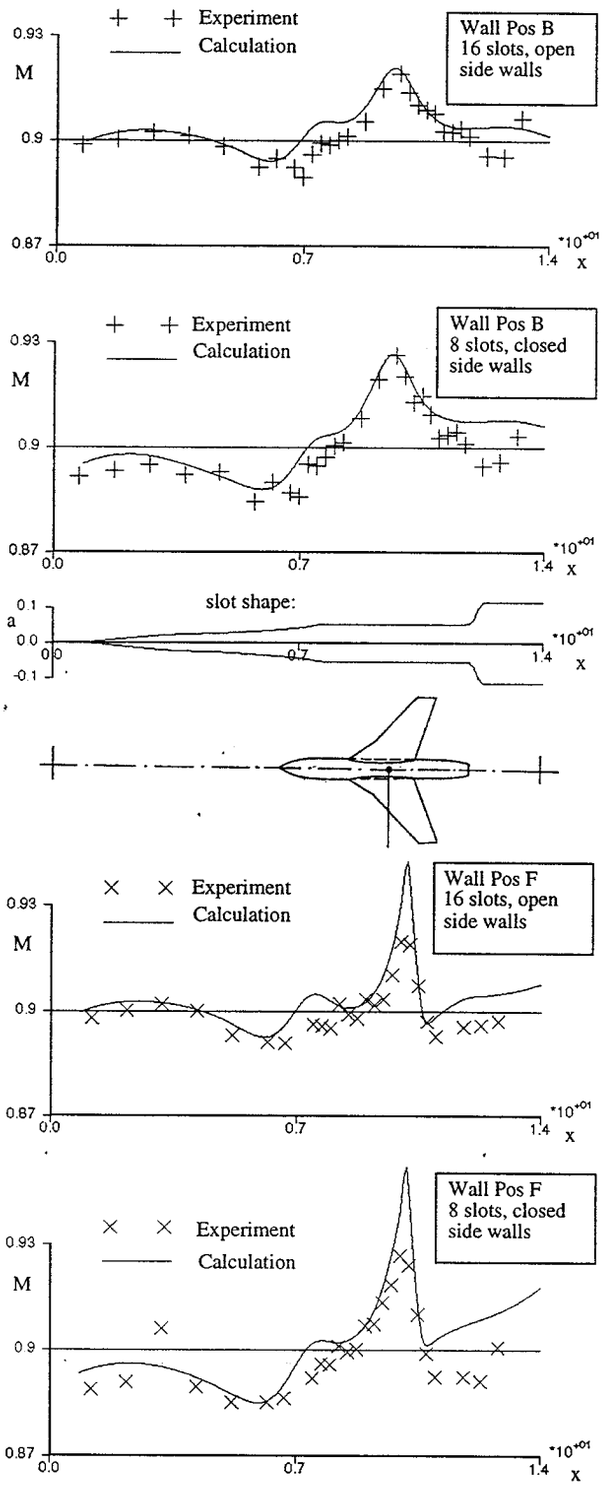

Figure 10 Wall Mach number distribution at Mach 0.9, $\alpha=1^{o}$ in TVM500. Comparison for open and closed side walls along postions B and F.

At the top of Figure 11 the differences between the slot fluxes of slot number 2 can be seen. It confirms the previous discussion that closing the side walls increases the slot fluxes.The plenum pressure surfaces are also shown with and without closing the walls. It can be observed that the lifting wing and its wake are turning the flow back into the test section. A bubble of quiscent plenum air is expanding into the test section from the rear part of the slot. Moreover, in the closed side wall case the returning inflow is slightly delayed compared to the open side wall case.

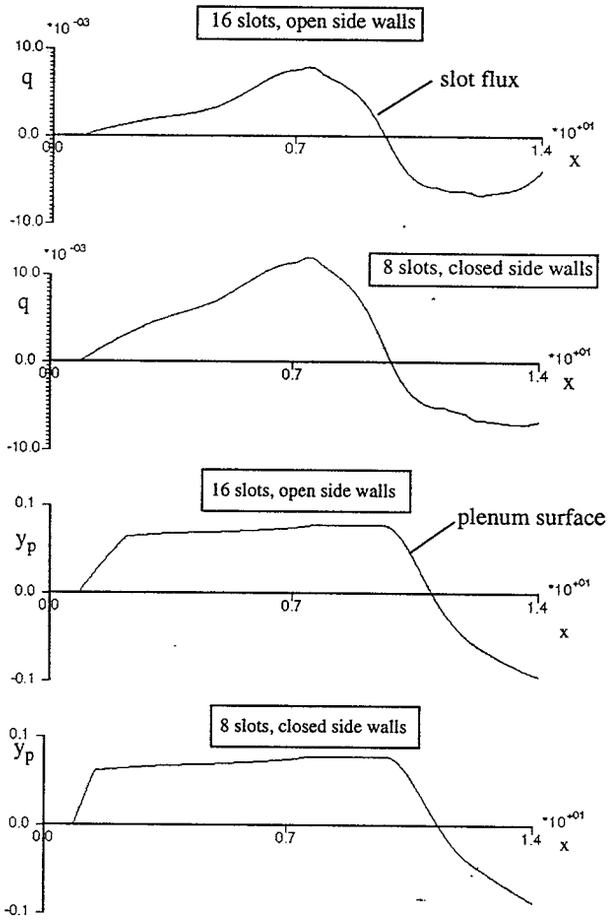

Figure 11 Slot fluxes and plenum pressure surfaces of slot No 2 with and without closing the side walls in TVM500. Mach =0.9, $\alpha=1^{o}$.

From Figure 10 one can see that the calculation overpredicts the local maximum wall Mach number along the side wall at position F, where the wing tip is close to the wall. The side wall is just 0.05 m away from the wing tip. The reason for this overshoot can be the potential flow equation with the wing wake located in a fixed plane position not separating or convecting naturally in the flow which should be the case with e.g. an Euler equation solver. Moreover, if there is a non-negligible aeroelastic twist it would relax the tip load thereby reducing the wing tip influence on the side wall.

Another feature that generally can be observed in the Mach calculations on the wall is that at the location of the nose part of the fuselage there is a tendency of a too quick local

overexpansion recovery in Mach number compared to experiments. Although there is a weak tendency of changing convexity in the Mach distribution in this region even in the experiments, the behaviour is too pronounced in the computations. The reason for this can be a bad numerical representation of the fuselage in this region, or the result of a stiff modeling of the influence of the slot width gradient da/dx in Eqs (2), (3). This comes from the simplified cross-flow massflow balance applied inside the slot where the boundary condition for the solid slot sides implies the terms with da/dx. An attempt to take into account also the streamwise massflow influence did not give any visible improvement. The peculier Mach behaviour was also observed in calculations presented e.g. in Ref (16) using a somewhat different transonic small perturbation equation. However, the solution to this seems likely to be revealed in Figure 12. In this figure the freestream and the tunnel simulation with 16 slots show very close agreement regarding the calculated wall Mach number M along the top wall, position B, of the TVM500.

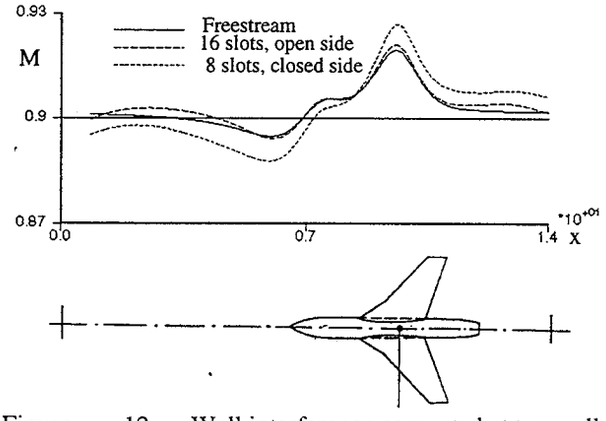

Figure 12 Wall interference computed at top wall along line B in TVM500. Mach comparison: Unbounded freestream, closed- and open side walls. Mach 0.9, $\alpha = 1^{\circ}$.

Hence, it can not be the slot flow model itself that is causing the local hump like behaviour located at the nose position of the fuselage. The same behaviour at this location for a completely different test model was in fact observed also in Ref (16) , although the conclusion there was pointing at the slot flow model. One likely explanation instead is that the physical flow model in terms of the potential equation is not sufficient to model the propagation of disturbances originating e.g. from a relatively blunt nose. A better physical flow model would be to use e.g. the Euler equations. This will be checked by running the freestream case with an Euler solver. The Euler equations would also ensure a natural convection and rolling up of the wing wake at the wing tip and downstream of the wing under the influence of the interacting walls. The present slot flow model has to be used in formulating an outer pressure boundary condition over the wall strips, see Figure 6, in much the same way as is presently done.

The computational input data for the Mach 0.9, $\alpha=1^{\circ}$ case, as illustrated in Figure 10, Figure 11 and Figure 12, were given by the measured plenum Mach number M_p for the corresponding chosen reference Mach number M_r labeling the experiment. In principle, the relation between them comes from empty tunnel calibrations. The slot flow viscous loss factors used for all slots were η_a=.78 and η_U=.87. They were estimated by making simple perturbation analysis of the slot flow equations in the two distinguished points mentioned earlier in the section explaining basic slot flow physics. A coupled two equation system gave the results by matching computations to measured wall Mach numbers along position B at the two mentioned point locations. The same figures were then used for all slots although this procedure could have been repeated. In the TVM500 testing the only active pressure taps were along postions B and F.

Comparison of calculations and measurements at Mach 0.8

Some further calculations were carried out to compare results with measurements at Mach 0.8. The wing pressure tap stations active in the TVM500 tests were at 60% and 92% of the half span of the wing.

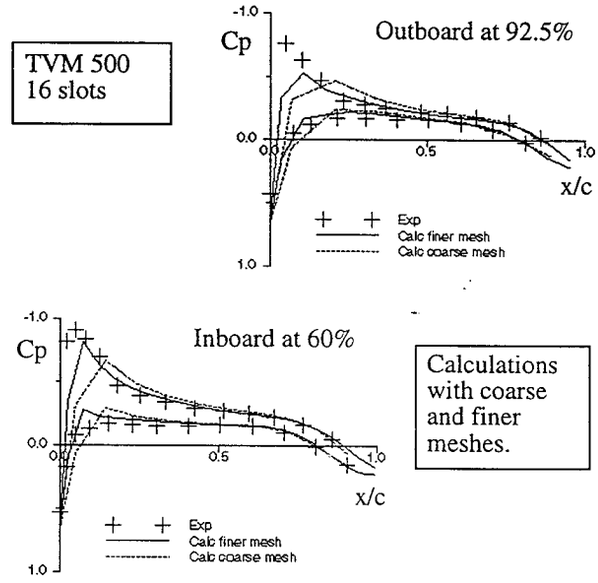

Figure 13 Calculated and measured wing pressure in TVM500 at half span stations 60% and 92.5% respectively. Mach 0.8, $\alpha=2^{\circ}$.

From the Cp-results of Figure 13 it is revealed that this kind of relatively blunt nosed swept leading edge wing can hardly be accurately modeled in the leading edge region. The rectangular Cartesian type of grid as presently used is not well suited. The thin wing boundary condition formulation and the number of grid points used seem insufficient. This also emhasizes the conclusion drawn in the previous

section about the local over expanding wall Mach distribution above the fuselage nose. However, further downstream behind the wing leading edge the agreement is very good between calculation and experiment. It was improved by the inclusion of a wing boundary layer of classical integral type.

In Figure 14 the wall Mach number distribution of the Mach 0.8 case, but now with angle of attack $\alpha = 4.89^{o}$, was considered.

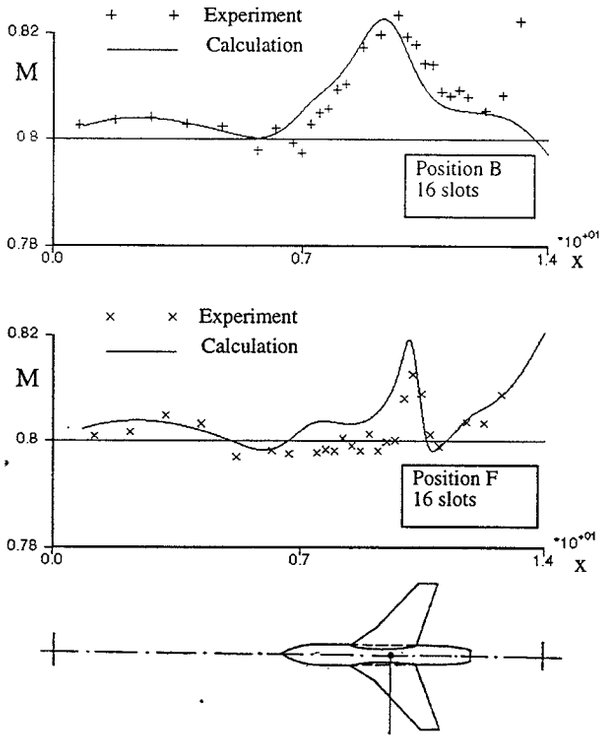

Figure 14 Wall Mach number in TVM500 at postions B and F with 16 slots. Mach 0.8, $\alpha = 4.89^{o}$.

The quality of agreement between calculations and measurements in Figure 14 is about the same as with the higher reference Mach number shown in Figure 10. The local over shoot expansion in the calculated wall Mach number where the nose is ending and joining the cylindrical part of the fuselage is still there. Moreover, the strong locally computed interaction on the side wall, where the local maximum Mach number on the wall at position F is, has not changed. However, it is somewhat weaker compared to Figure 10. In the present calculations the tunnel setting was used as in the experiment. The loss factors were the same as applied in the previously presented Mach 0.9 run case. Perturbation analysis of the slot flow equations with input from the measured and calculated wall Mach numbers could have given individual values for each slot although this analysis was not carried out during this study.

In Figure 15, Figure 16 and Figure 17 integrated forces are compared. Connected symbols indicate calculations. The same symbols are used for corresponding calculations and experiments. In Figure 15 the lift $C_L(\alpha)$ is shown for tests in the TVM500 as well as in the T1500 and matched by corresponding simulations and calculated unbounded freestream case. Calculations were done up to about $\alpha = 5^{o}$. Similar evaluations were carried out for the pitching moment C_m (C_L) in Figure 16 and the drag $C_D(C_L^2)$ in Figure 17. Some experimental results are shown for $\alpha > 5^{o}$.

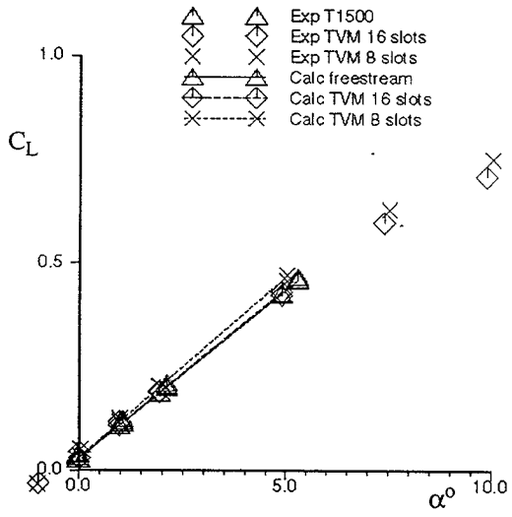

Figure 15 Lift force C_L comparison vs angle of attack α. Calculations contra experiments in T1500 & TVM500. Number of slots in TVM500 is 16 and 8 respectively. In T1500 16 slots. Reference Mach 0.8 .

Looking at Figure 15 the computed lift force is in very good agreement with experiments for all considered cases. The T1500 data is in good agreement with calculated freestream as it should be with the test-model being very small in that test section. The known trend between a more open and closed test section is computationally resolved in the calculated results in the TVM500 with 16 slots and 8 slots respectively. It is encouraging that a big model in the small TVM500, blocking 1.7% of the cross section and spanning the tunnel width to 80%, gives such close agreement with the same model in T1500 where the blocking is 0.2% and the span is 27% of the width.

In Figure 16 the pitching moment C_m versus C_L is shown. The zero pitching moment at $C_L=0$ is not well predicted in the present calculations. However, it can be observed that the static stability margin, dC_m/dC_L, is in rather good agreement with experimental data. Here the case with 16 slots in the TVM500 seems to give good agreement with experimental data. The calculated freestream and the calculated 16 slot TVM500 case indicate only small differences in the slope dC_m/dC_L.

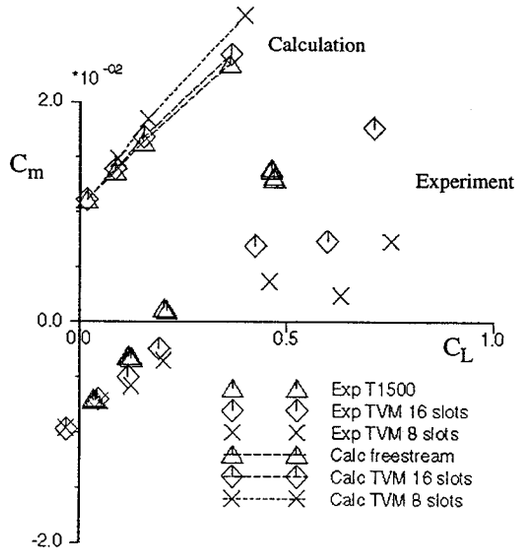

Figure 16 Pitching moment *Cm* vs C_L. Calculations contra experiments in T1500 & TVM500. Number of slots in TVM500 is 16 and 8 respectively. In T1500 16 slots. Reference Mach 0.8 .

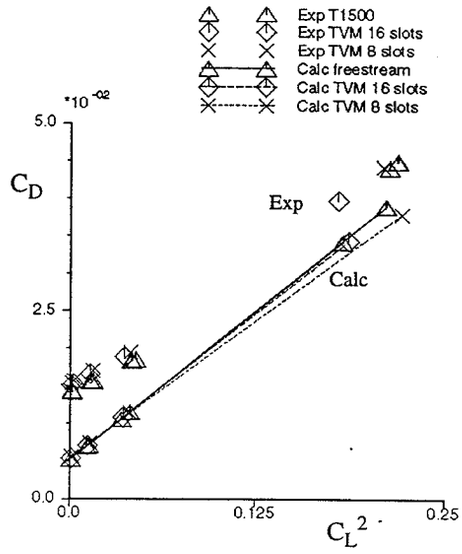

Figure 17 Drag C_D vs C_L^2 . Calculations contra experiments in T1500 & TVM500. Number of slots in TVM500 is 16 and 8 respectively. In T1500 16 slots. Reference Mach 0.8 .

Finally, in Figure 17 the drag results are shown and plotted as C_D versus C_L^2. The level of the computed zero lift drag value is not representative as the friction drag is not included. An estimate of the friction drag indicates a finally friction corrected zero lift drag value that is higher than the measured with about 30%. This emphasizes the delicate accuracy problem at wing leading edges and blunt nose tips within the context of small perturbation modeling. Looking at the slope dC_D/dC_L^2 , which is connected with the lift dependent drag, the computational simulation is in good agreement with experiments. The experimental data is less linear as function of C_L^2 close to $C_L=0$ because the minimum of the drag polar is shifted a bit outside the position where $C_L=0$. Regarding the slope dC_D/dC_L^2 the calculated freestream results agree very well with the tests in the T1500. The computed case in TVM500 with solid side walls agrees with the corresponding tests in the linear part of the graph.

Comments on the results

Generally, the results from this study are encouraging and it is interesting that models of this size as used in the small TVM500 did not experience more wall interference than shown at the considered Mach number.

The slot flow model as used in this investigation works properly. It can be improved on some points but it gives the correct physical behaviour and the idea of discrete slot interaction seems worthwhile to follow. Many aspects of the integrated forces on the test model are computationally well described using the small perturbation equation in the considered test cases.

However, there are latent problems with locally blunt configurations where the small perturbation assumption breaks down. This needs further attention in terms of grid resolution, gridpoint distributions and the way of how the boundary conditions on the test model are being applied. A sheared Cartesian or a body conform grid would probably improve on the situation.

The complexity in terms of computer resources and CPU time will increase by switching over to e.g. the Euler equations inside the test section. For complicated flows this is likely to be necessary. Trailing wakes behind wings will then naturally convect and separate under the influence from the test section walls.

Conclusions

The present slot flow model seems to be accurate enough for discrete slot applications in rectangular slotted-wall test sections. It is suitable for repeated use forming an iterative numerical boundary condition to the inner field equation describing the flow around the test object. For less complex flows or qualitative investigations, it may be sufficient to use the small perturbation equation solved on a Cartesian grid inside the test section. From many aspects good results have been shown in this study. An encouraging finding from the present investigation is the indication of correctability for wall interference even for models spanning up to 80% of the width of the test section.

Acknowledgement

The authors want to thank *The Swedish Defense Material Administration FMV* and the *Saab AB* company for supporting this research. Without the long term funding from *FMV* this research would have been impossible.

References

1. Berndt, S.B. Sörensen H., Flow properties of slotted walls for transonic test sections, AGARD Conf Proc No 174, Paper No 17, 1975.
2. Berndt, S.B. Inviscid theory of wall interference in slotted test sections. AIAA J. Vol 15, Sept 1977, pp 1278-1297.
3. K.R. Karlsson, Y.C-J.Sedin, Axisymmetric calculations of transonic wind tunnel interference in slotted test sections. AIAA J.,Vol 17, No 8, 1979, pp 917-919.
4. K.R. Karlsson, Y.C-J.Sedin, Numerical design and analysis of optimal slot shapes for transonic test sections - Axisymmetric flows. AIAA J. of Aircraft, Vol 18 No 3, March 1981, pp 168-175.
5. Y.C-J. Sedin, K.R. Karlsson, Some theoretical wall-interference calculations in slotted transonic test sections, Three-dimensional flows. 13th ICAS Congress, Seattle, Wash., USA, Aug 1982.
6. Y.C-J. Sedin, N.Agrell, N.Zang, A local slot boundary condition for transonic flow calculations in slotted-wall test sections of wind tunnels. FFA TN 1984-34, Stockholm 1984.
7. Y.C-J Sedin, N.Agrell, N.Zang, Computation of transonic wall-interference in slotted-wall test sections of wind tunnels. Proc. of the Int. Symp. on Computational Fluid Dynamics-Tokyo, Tokyo, Sept 1985 (Oct 1986, Japan Soc. of Comp. Fluid Dyn.).
8. Y.C-J Sedin, H. Sörensen, Computed and measured wall interference in a slotted transonic test section. AIAA J., Vol 24, No 3, March 1986, pp 444-450.
9. N.Agrell, B.Pettersson, Y.C-J. Sedin, Numerical design parameter study for slotted walls in transonic wind tunnels. 15th ICAS Congress, London 1986.
10. N.Agrell, B. Pettersson, Y.C-J. Sedin, Numerical computations and measurements of transonic flow in a slotted-wall wind tunnel. AIAA 5th Appl. Aerod. Conference, Monterey, Cal., USA, 1987.
11. Y.C-J. Sedin, Slotted-wall theory for rectangular test sections with reference to optimal slot design. Part 1-Theory. FFA TN 1988-07.
12. Y.C-J. Sedin, N. Zang, N. Agrell, B. Pettersson, Slotted-wall theory for rectangular test sections with reference to optimal slot design. Part 2-Numerical applications in transonic flow. FFA TN 1988-10.
13. Y.C-J. Sedin, N.Zhang, N.Agrell and B.Pettersson. Numerical design and analysis of slotted-walls in a rectangular transonic test-section. Proc.: Conf. on Adaptive Wall Wind Tunnel Research and Wall Interference Correction. Xian, Shaanxi, China , June 1991.
14. Agrell, N. , Computational simulations for some tests in transonic wind tunnels. AGARD, 73rd Fl. Dyn. Panel Mtg and Symp. on Wall Interference and Flowfield Measurements. Paper No 14, Brussels Oct 1993.
15. M.L. Rueger, R.C. Crites, R.F. Weirich, F. Creasman, R.K. Agarwal, J.E. Deese, Transonic Wind Tunnel Boundary Interference Correction, AGARD Conference Proceedings 535, 1993.
16. J. A. Al-Saadi, Wall interference and boundary simulation in a transonic wind tunnel with a discretely slotted test section. NASA TP 3334, Sept 1993.
17. N. Agrell, W. Fritz, S. Hedman, W. Schmidt, Berechnung und Entwurf Flugel-Rumpf Kombinationen in transonischer Strömung unter Berucksichtigung endlicher Rumpfe. Dornier Bericht 76/42B, 1976.